Monthly Notices
of the
ROYAL ASTRONOMICAL SOCIETY

MNRAS **470,** 4241–4250 (2017)
Advance Access publication 2017 June 13

doi:10.1093/mnras/stx1467

DES15E2mlf: a spectroscopically confirmed superluminous supernova that exploded 3.5 Gyr after the big bang

Y.-C. Pan,[1★] R. J. Foley,[1] M. Smith,[2] L. Galbany,[3,4] C. B. D'Andrea,[2,5] S. González-Gaitán,[6,7] M. J. Jarvis,[8,9] R. Kessler,[10,11] E. Kovacs,[12] C. Lidman,[13] R. C. Nichol,[5] A. Papadopoulos,[5,14] M. Sako,[15] M. Sullivan,[2] T. M. C. Abbott,[16] F. B. Abdalla,[17,18] J. Annis,[19] K. Bechtol,[20] A. Benoit-Lévy,[17,21,22] D. Brooks,[17] E. Buckley-Geer,[19] D. L. Burke,[23,24] A. Carnero Rosell,[25,26] M. Carrasco Kind,[27,28] J. Carretero,[29,30] F. J. Castander,[29] C. E. Cunha,[23] L. N. da Costa,[25,26] S. Desai,[31] H. T. Diehl,[19] P. Doel,[17] T. F. Eifler,[32] D. A. Finley,[19] B. Flaugher,[19] J. Frieman,[10,19] J. García-Bellido,[33] D. A. Goldstein,[34,35] D. Gruen,[23,24] R. A. Gruendl,[27,28] J. Gschwend,[25,26] G. Gutierrez,[19] D. J. James,[16,36] A. G. Kim,[35] E. Krause,[23] K. Kuehn,[13] N. Kuropatkin,[19] O. Lahav,[17] M. Lima,[25,37] M. A. G. Maia,[25,26] M. March,[15] J. L. Marshall,[38] P. Martini,[39,40] R. Miquel,[30,41] P. Nugent,[34,35] A. A. Plazas,[32] A. K. Romer,[42] E. Sanchez,[43] V. Scarpine,[19] M. Schubnell,[44] I. Sevilla-Noarbe,[43] R. C. Smith,[16] F. Sobreira,[25,45] E. Suchyta,[46] M. E. C. Swanson,[28] R. C. Thomas,[35] A. R. Walker[16] and (The DES Collaboration)

Affiliations are listed at the end of the paper

Accepted 2017 June 8. Received 2017 June 8; in original form 2017 January 3

ABSTRACT

We present the Dark Energy Survey (DES) discovery of DES15E2mlf, the most distant superluminous supernova (SLSN) spectroscopically confirmed to date. The light curves and Gemini spectroscopy of DES15E2mlf indicate that it is a Type I superluminous supernova (SLSN-I) at $z = 1.861$ (a lookback time of ∼10 Gyr) and peaking at $M_{\rm AB} = -22.3 \pm 0.1$ mag. Given the high redshift, our data probe the rest-frame ultraviolet (1400–3500 Å) properties of the SN, finding velocity of the C III feature changes by ∼5600 km s^{-1} over 14 d around maximum light. We find the host galaxy of DES15E2mlf has a stellar mass of $3.5^{+3.6}_{-2.4} \times 10^9$ M$_\odot$, which is more massive than the typical SLSN-I host galaxy.

Key words: supernovae: general – supernovae: individual: DES15E2mlf.

1 INTRODUCTION

In the era of untargeted wide-field sky surveys, thousands of supernovae (SNe) are discovered each year, uncovering many new classes of SNe. Among these, superluminous supernovae (SLSNe; Gal-Yam 2012), being 10–100 times as bright as typical Type Ia SNe (SNe Ia) and core-collapse SNe (CCSNe), are particularly interesting. SLSNe are relatively rare, having a rate <0.1 per cent that of the CCSN rate (e.g. Quimby et al. 2013; McCrum et al. 2015; Prajs et al. 2017). Given their high luminosities, SLSNe are detectable to higher redshifts compared with SNe Ia and CCSNe (e.g. $z \gtrsim 1.5$; Berger et al. 2012; Cooke et al. 2012; Howell et al. 2013).

There is significant debate about what powers SLSNe. Several models have been proposed to explain the extremely high luminosities of these events. For instance, the SN luminosity could be primarily powered by the spin-down of a newborn magnetar, where the rotation energy is deposited into the SN ejecta (Kasen & Bildsten 2010; Woosley 2010). Alternatively, the release of shock energy by collision with an opaque circumstellar material (CSM; Chevalier & Irwin 2011; Ginzburg & Balberg 2012), or the explosion of pair-instability supernova (PISN; Barkat, Rakavy & Sack 1967) could power the high luminosity.

★ E-mail: ypan6@ucsc.edu

Gal-Yam (2012) divided SLSNe into three different sub-classes: SLSN-I, SLSN-II and SLSN-R, based on either their spectroscopic or photometric properties. SLSNe-II have strong, narrow hydrogen emission lines in their spectra, which are believed to be caused by the interaction with hydrogen-rich CSM (e.g. Smith et al. 2007). SLSNe-R have a slow luminosity decay, consistent with being powered by ^{56}Co decay, a predicted outcome of pair-instability models (e.g. Gal-Yam et al. 2009).

Compared to SLSNe-II, SLSNe-I are characterized by the lack of hydrogen features in their spectra and exceptionally high peak luminosities (Quimby et al. 2011). The spectra at early phases are usually featureless in the optical region with most of the flux and absorption features found in the ultraviolet (UV; e.g. Chomiuk et al. 2011; Quimby et al. 2011; Howell et al. 2013; Vreeswijk et al. 2014; Papadopoulos et al. 2015; Smith et al. 2016). These events show some spectral similarities with broad-line Type Ic SNe, but require an additional energy source beyond that of standard CCSNe (e.g. Inserra et al. 2013; Nicholl et al. 2013).

Previous studies have found that SLSNe-I exclusively reside in faint, low-mass ($M_{\rm stellar} < 10^{10}\,{\rm M}_{\odot}$) galaxies (Neill et al. 2011; Chen et al. 2013; Lunnan et al. 2013, 2014; Chen et al. 2015; Leloudas et al. 2015). For the subset of host galaxies having spectroscopic metallicity measurements, all have low gas-phase metallicities. Similarly, SLSN host galaxies have high specific star formation rates (sSFR), making them similar to the host galaxies of long-duration gamma-ray bursts (Leloudas et al. 2015, although it is possible that the SLSN progenitor star populations are even *younger*). The low metallicity environments have been interpreted as being critical for the formation of SLSNe and are used as a distinguishing characteristic for models (e.g. Perley et al. 2016).

The Dark Energy Survey supernova program (DES-SN; Bernstein et al. 2012) has discovered ∼20 SLSNe and identified many additional SLSNe candidates since 2013 (Papadopoulos et al. 2015; Dark Energy Survey Collaboration et al. 2016; Smith et al. 2016). Here, we present DES15E2mlf, another interesting SLSN at $z = 1.861$ discovered by the DES-SN. DES15E2mlf is the highest redshift spectroscopically confirmed SLSN, providing unique insight into the UV properties and possible redshift evolution of SLSNe. The plan of the paper is as follows. In Section 2, we describe the discovery and observations of DES15E2mlf. Section 3 presents the analyses of the photometry, spectroscopy and host galaxy. We discuss our findings in Section 4 and conclude in Section 5. Throughout this paper, we assume $H_0 = 70$ km s^{-1} Mpc^{-1} and a flat universe with $\Omega_{\rm M} = 0.3$.

2 DISCOVERY AND OBSERVATIONS

DES15E2mlf was discovered in exposures taken by DES on 2015 November 7 (UT) at $\alpha = 00^{\rm h}41^{\rm m}33\overset{\rm s}{.}40$, $\delta = -43^{\circ}27'17\overset{''}{.}20$ (Pan et al. 2015). It is located in the 'E2' shallow field, one of the 10 SN fields (two deep and eight shallow fields) in DES-SN. The SN was detected with the difference imaging pipeline (Kessler et al. 2015). The light curves were observed in the DECam (Flaugher et al. 2015) *griz* filters over ∼2 months. DES15E2mlf was followed by the DES through the end of the observing season (Diehl et al. 2016) in February 2016. The DECam images were reduced using the same photometric pipeline, as described in Papadopoulos et al. (2015) and Smith et al. (2016). We subtract a deep template image from each SN image to remove the host-galaxy light using a point spread function (PSF) matching routine. We then measure the SN photometry by fitting its PSF from the difference image. The light curves of DES15E2mlf are shown in Fig. 1.

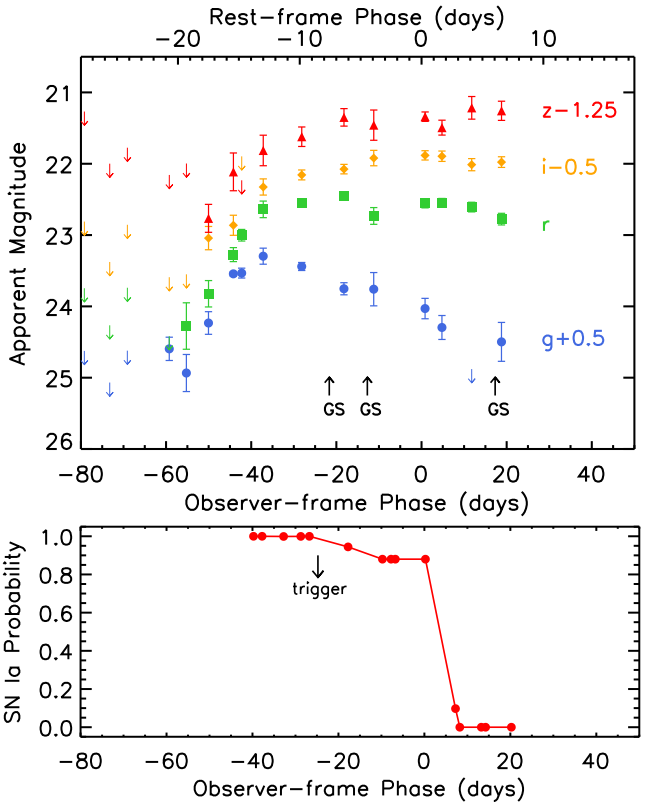

Figure 1. Top panel: DECam *griz* light curves of DES15E2mlf. The phase of observation is relative to the peak of the *i*-band light curve on MJD = 57384.26. Upper limits are represented by the downward arrows. The upward arrows in black mark the epochs of Gemini-South spectra. Bottom panel: PSNID (Sako et al. 2008, 2011) probability of DES15E2mlf being an SN Ia as a function of phase. The arrow indicates the epoch when we triggered the first spectrum.

At discovery, the SN was ∼1.2 mag below peak in the *i* band. From discovery, the SN rose in all bands. In fact, the SN was discovered 49 d (17 rest-frame days) before peak (see Section 3.4). Despite its proximity to its host galaxy (offset by 0.1 arcsec from the nucleus), its relatively bright luminosity (∼1 mag brighter than its host) made DES15E2mlf a good candidate for spectroscopic observations.

Intriguingly, DES15E2mlf was not initially flagged as a potential SLSN. Rather, its early light curves were similar to SN Ia light curves at $z \approx 0.3$. Complicating the proper identification was the fact that its host galaxy has a photometric redshift of 0.343 ± 0.103 estimated from the DECam *griz* photometry (Bonnett et al. 2016), consistent with the implied SN redshift. However, the photometric redshift is way off from the redshift measured from the host features in the SN spectrum (see Section 3.1). We found this incorrect photometric redshift of the host galaxy is likely due to the lack of rest-frame optical photometry (see Section 3.5 for more details).

In the bottom panel of Fig. 1, we display the probability that DES15E2mlf was an SN Ia as determined by the PSNID software (Photometric SN IDentification; Sako et al. 2008, 2011) as a function of phase. It was consistently considered a likely SN Ia until after peak brightness when the colours became inconsistent with that of an SN Ia. Although DES15E2mlf was considered highly

unlikely an SN Ia at that point, PSNID was unable to classify it as an SLSN due to the lack of SLSN templates.

Based on its initial classification as a likely SN Ia with an SN redshift consistent with its host-galaxy photometric redshift, we triggered spectroscopic follow-up observations through our SN Ia program with Gemini-South (program GS-2015B-Q-7; PI Foley). This first spectrum was obtained on 2015 December 6. The observations consisted of 3 × 1200 s exposures taken with the Gemini Multi-Object Spectrograph (GMOS; Hook et al. 2004) using the R400 grating and a central wavelength of 750 nm (observed wavelength range of ∼5200–9900 Å). We selected an angle to place the centre of slit (with 1 arcsec slit width) through both the SN and the host-galaxy nucleus.

The data reduction process included standard CCD processing and spectrum extraction with IRAF.[1] We applied our own IDL routines to flux calibrate the data and remove telluric lines using the well-exposed continua of the spectrophotometric standard stars (Wade & Horne 1988; Foley et al. 2003). Details of the spectroscopic reduction are described in Silverman et al. (2012).

To investigate the potential spectral evolution, two more Gemini/GMOS spectra were obtained on 2015 December 15, (program GS-2015B-Q-8; PI Galbany) and 2016 January 14 (program GS-2015B-Q-7; PI Foley), respectively. The December observations used both the R400 configuration and an additional configuration with the B600 grating (observed wavelength range of ∼3800–7000 Å) for a total wavelength range of ∼3800–9900 Å. The January spectrum only utilized the B600 grating. Two additional spectra were obtained with the AAOmega Spectrograph (Saunders et al. 2004) and the 2dF fibre positioner at the Anglo-Australian Telescope (AAT) on December 12 and 14. However, other than noting that the continuum of DES15E2mlf was conspicuously blue, the signal-to-noise ratio of the AAT spectra are too low (S/N $\lesssim$ 1) to confidently identify either SN or host galaxy features. Thus, in this work, wepresent only an analysis of the Gemini spectra. The whole spectral sequence and log of spectroscopic observations can be found in Fig. 2 and Table 1 , respectively.

3 DATA AND ANALYSIS

3.1 Redshift

In Fig. 2, we present the Gemini spectra of DES15E2mlf at phases of −8, −4 and +6 d (in the rest frame) relative to *i*-band maximum brightness. There are clear narrow absorption features in the spectra of DES15E2mlf. We identify the most prominent lines as the Mg II λλ2796, 2804 doublet at $z = 1.8607 \pm 0.0003$ (see Fig. 3). We find no significant evolution of the absorption lines for the phases covered by our spectra. Following Berger et al. (2012), we compare the continuum-normalized spectra of DES15E2mlf to the Christensen et al. (2011) Gamma-ray burst (GRB) composite spectrum in Fig. 3. Also marginally detected (∼2σ significance) in the spectra are Fe II λλ2374, 2383 and Fe II λ2600 lines, although they are much weaker than the Mg II doublet. There are no other obvious absorption features at other redshifts. At this redshift, DES15E2mlf is also consistent with that of hydrogen-poor SLSNe-I (see Section 3.3).

[1] The Image Reduction and Analysis Facility (IRAF) is distributed by the National Optical Astronomy Observatories, which are operated by the Association of Universities for Research in Astronomy, Inc., under cooperative agreement with the National Science Foundation.

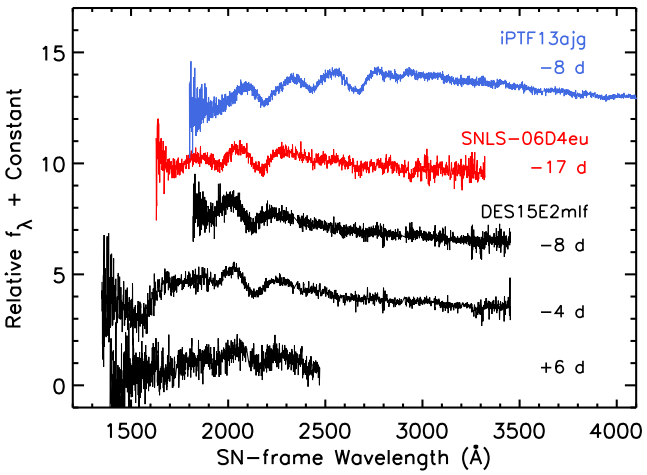

Figure 2. Gemini-South spectra of DES15E2mlf (black) at −8, −4 and +6 d relative to peak *i*-band brightness. We also display the spectra of iPTF13ajg (blue), and SNLS-06D4eu (red) and SLSNe-I at $z = 0.740$ and 1.588, respectively.

Table 1. Log of spectroscopic observations of DES15E2mlf.

Date (MJD)	Instrument	Grating	Exposure time (s)
57362.59	Gemini-S/GMOS[a]	R400	3600
57371.53	Gemini-S/GMOS[b]	B600/R400	3600/1800
57401.55	Gemini-S/GMOS[a]	B600	4800

[a]The spectra were observed under GS-2015B-Q-7 (PI Foley).
[b]The spectra were observed under GS-2015B-Q-8 (PI Galbany).

3.2 Classification

Examining the spectra, we find that DES15E2mlf is most similar to hydrogen-poor SLSNe-I. However, our spectra do not cover the wavelengths of any hydrogen lines, and therefore, we cannot definitively rule out the possibility of DES15E2mlf being an SLSN-II. None the less, based on the spectra alone, the best classification is that of an SLSN-I.

Further supporting the SLSN classification is its peak luminosity. DES15E2mlf had a peak apparent AB magnitude of $i = 22.4 \pm 0.1$ mag ($\lambda_{\rm rest} \approx 2745$ Å). Correcting for minimal Milky Way extinction ($A_i = 0.02$ mag; Schlafly & Finkbeiner 2011) and cosmic expansion, DES15E2mlf peaks at $M_{\rm AB} = -22.3 \pm 0.1$ mag. At this luminosity, DES15E2mlf is well above the (arbitrary) SLSN threshold ($M < -21$ mag; Gal-Yam 2012).

Cooke et al. (2012) reported two SLSNe at $z = 2.05$ and 3.90, respectively. However, the lack of solid spectroscopic observations made the classification uncertain and questionable. At $z = 1.861$, DES15E2mlf is the most distant spectroscopically confirmed SLSN that exploded only 3.5 Gyr after the big bang.

3.3 Spectra

The multiple spectra of DES15E2mlf show two strong absorption features at rest-frame wavelengths of ∼1950 and 2150 Å, respectively. No strong features are found between 2300 and 3500 Å. The spectra are similar to those of other SLSNe, and, in particular, to that of SNLS-06D4eu (see Fig. 2), however, DES15E2mlf has the absorption features shifted further to the blue, with even the latest spectrum of DES15E2mlf being further to the blue by ∼1800 km s^{-1} than the −17-day spectrum of SNLS-06D4eu.

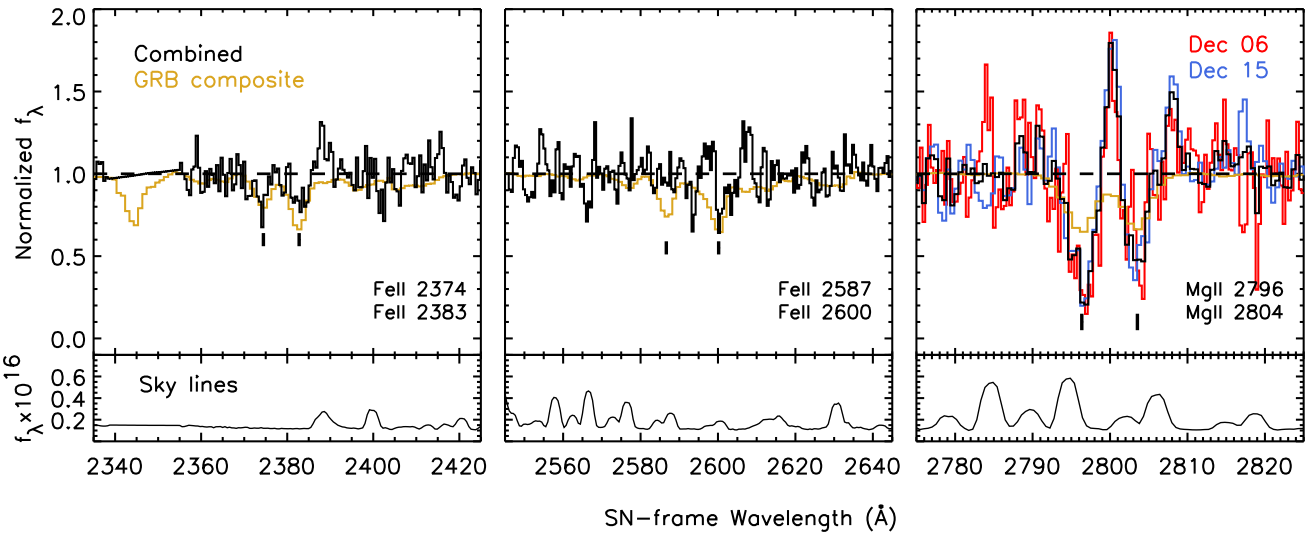

Figure 3. Upper panel: Continuum-normalized spectra of DES15E2mlf near the Fe II (left-hand and middle panels) and Mg II (right-hand panel) doublets. Each line is marked. The December 6 and 15 spectra are shown as blue and red curves, respectively. The combined spectrum is shown in black. The GRB composite spectrum from Christensen et al. (2011) is shown in gold. Lower panel: The spectrum of extracted sky emission lines.

However, it is still smaller than the typical expansion velocity an SLSN may have (∼10 000–20 000 km s^{-1}; e.g. Inserra et al. 2013; Mazzali et al. 2016). Here, the velocity is calculated by first deredshifting and smoothing the spectrum using an inverse-variance-weighted Gaussian filter. We then use the wavelength of the maximum absorption in the smoothed spectrum to calculate the velocity (see Blondin et al. 2006, for more details). Mazzali et al. (2016) identified the absorption features as Fe III and C III, respectively. In Fig. 2, we also compare the spectrum to that of iPTF13ajg, an SLSN-I at $z = 0.74$. We found both high-redshift DES15E2mlf and SNLS-06D4eu lack some spectral features (or they could be relatively weak) seen in iPTF13ajg, particularly the 2700 Å line (mostly resulting from Mg II), which was commonly found in many of low-redshift SLSNe.

Given the high redshift of DES15E2mlf, our multiple optical spectra probe the far-UV spectral evolution of an SLSN. In Fig. 4, we display the spectra of DES15E2mlf from −8 to +6 d relative to peak brightness, focusing on the absorption features identified above. Here, we investigate the velocity evolution of DES15E2mlf, but we describe any velocity changes relative to the first spectrum so as to not assume a particular rest-frame wavelength.

Over the time covered by our spectra, the ∼2150 Å feature (identified as C III) was redshifted by 5600 km s^{-1}. The ∼1950 Å feature (identified as Fe III) is not strongly detected in our third spectrum. However, between the first two epochs (−8 and −4 d), the feature was redshifted by 2800 km s^{-1}. We present this evolution in Fig. 4. A similar trend was found in other SLSNe (e.g. iPTF13ajg; Vreeswijk et al. 2014). Assuming that the 2150 Å feature is predominantly caused by the C III line (with a rest wavelength of 2297 Å), we calculate an expansion velocity of ∼22 600, 21 800 and 17 400 km s^{-1} at phases of −8, −4 and +6 d, respectively. This velocity evolution is consistent with those found from other SLSNe.

While the velocity of the strong absorption features changed significantly during the time period covered by our spectral observations, no significant change is found in the equivalent widths (EWs) of those features (Fig. 4). However, we are aware that there is possibly some host-galaxy contamination on our spectra that could affect the velocity and EW measurement. This effect should be small given that our spectra were observed when the SN light was still dominant (more than 1 mag brighter than the host galaxy). We test this by determining the best-fitting SED model of the host galaxy given by Z-PEG (see Section 3.5) and subtracting that from the SN spectrum. We found that the host-galaxy contamination has negligible effect on our results.

3.4 Light curves

In Fig. 1, we present the DECam *griz* light curves of DES15E2mlf (which have central wavelengths corresponding to $\lambda_{\rm rest} = 1700$, 2259, 2745 and 3215 Å in the rest frame, respectively). We fit a polynomial to each light curve to determine the peak luminosity and time of maximum brightness. We find that the SN had a peak *i*-band magnitude of 22.38 ± 0.07 mag on MJD $= 57384.26 \pm 0.08$. Here, the uncertainties of peak magnitude and MJD are computed by simply propagating the 1σ error of the *i*-band magnitude in the polynomial fit, and assuming the epochs of those measurements all have zero errors. The light curve rose for 62 observer-frame days to peak (in *i* band), corresponding to a rest-frame rise time of 21.5 d, comparable to that of SNLS-06D4eu (∼30 d). The time of maximum is later for redder bands. That is, the *grz* light curves peak −35, −23 and +3 observer-frame days (−12, −8 and +1 rest-frame days) relative to that of *i*-band, respectively.

While the *riz* light curves have a similar appearance, the *g*-band light curve evolves differently. Specifically, the *g* band (rest frame 1700 Å) reaches peak brightness much earlier than the other filters and then declines much faster than the other bands, decreasing ∼1 mag in 14 rest-frame days. The *g*-band light curve of DES15E2mlf probes bluer wavelengths than most previous SLSN-I light curves. Its rapid evolution compared to other bands may suggests unique information (e.g. SN cooling) at these wavelengths. However, the lack of early-time spectra (in *g* band) prevents us from making an explicit interpretation on our results.

In Fig. 5, we compare the absolute magnitude light curves of DES15E2mlf with those of SNLS-06D4eu, an SLSN at $z = 1.588$ (Howell et al. 2013). The absolute magnitudes for both SNe are determined by only correcting for the Milky Way extinction and cosmological expansion (e.g. equation 1 in McCrum et al. 2014). No proper *K*-correction is applied here. Since DES15E2mlf and

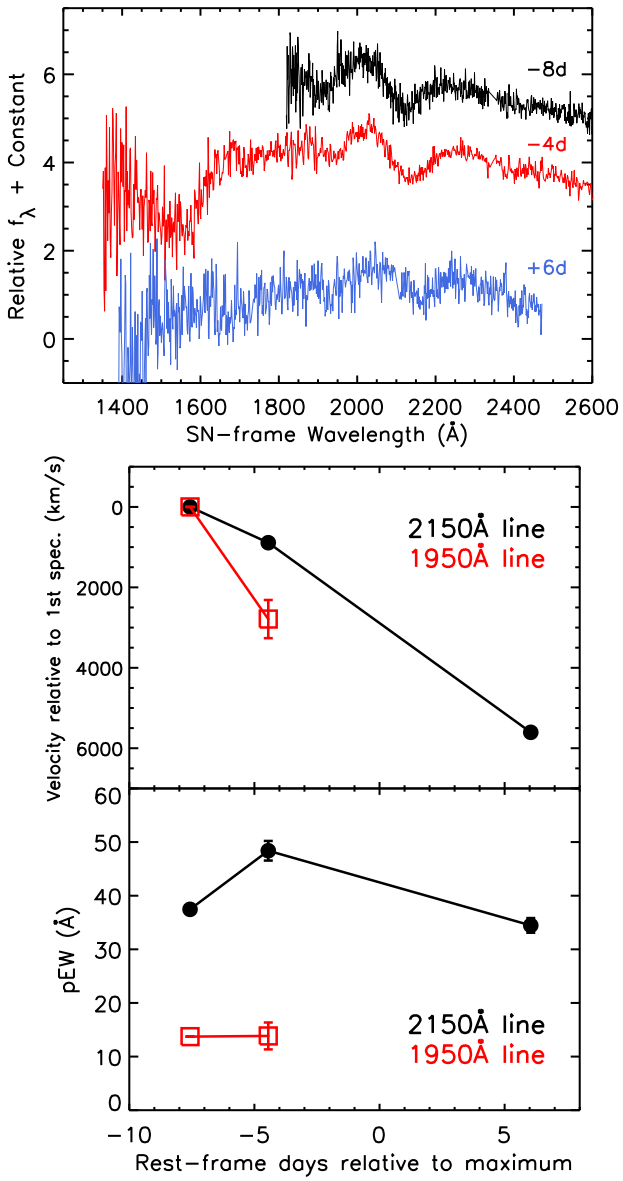

Figure 4. Top panel: Spectra of DES15E2mlf focusing on the two strong absorption features at ∼1950 and 2150 Å. Middle panel: Velocity of the 2150 Å (black circles) and 1950 Å (red open squares) absorption lines relative to the velocity in the first epoch as a function of phase. Bottom panel: Pseudo-equivalent width (pEW) for the two features as a function of phase.

SNLS-06D4eu have somewhat similar redshifts, the rest-frame effective wavelength for the *griz* filters are similar, making direct comparisons reasonable and simpler. Also compared is the *g*-band light curve of PS1-11ap, a well-studied SLSN at lower redshift ($z = 0.524$; McCrum et al. 2014). The *g* filter of PS1-11ap has a similar rest-frame wavelength (3193 Å) as that for the *z* filter of DES15E2mlf, providing a good comparison to our near-UV data.

DES15E2mlf has higher peak luminosities than those for SNLS-06D4eu at all bands, with the largest difference of 0.9 mag in *g*. The two SNe evolve similarly in *i* and *z* (corresponding to roughly 2850 and 3210 Å in the rest frame) for the range where both SNe have data. However, DES15E2mlf peaks later and has a slower decline in *g* (∼1840 Å in the rest frame) and *r* (∼ 2330 Å in the rest frame). While the exact timing and decline rate are different for the two

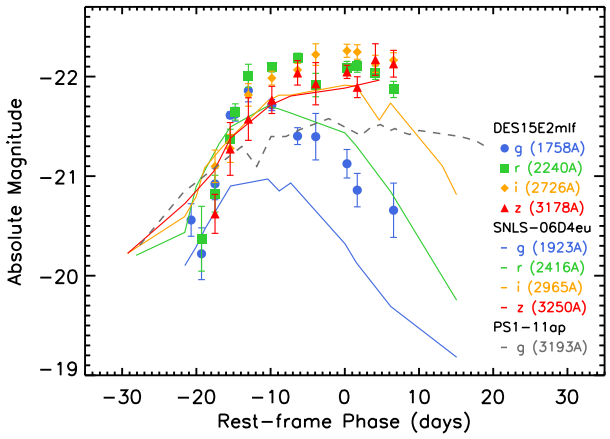

Figure 5. Absolute-magnitude light curves of DES15E2mlf (solid symbols), the $z = 1.588$ SLSN-I SNLS-06D4eu (solid lines; Howell et al. 2013) and the $z = 0.524$ SLSN-I PS1-11ap (dashed lines; McCrum et al. 2014). The *griz* bands are labelled with their rest-frame effective wavelength for each SN.

SNe in *g*, both have the same basic behaviour of peaking earlier and declining faster in *g* than in the other bands. The combination of a slower rise, slower decline, and generally higher peak luminosity in each band means that the integrated luminosity was larger for DES15E2mlf than SNLS-06D4eu (at least over the time when both SNe have data). The lower redshift PS1-11ap shows similar evolution in *g* (matches the *z*-band rest-frame wavelength of DES15E2mlf and SNLS-06D4eu), but has the lowest peak luminosity among all the SNe (∼0.5 mag lower than that of DES15E2mlf).

3.5 Host galaxy

Previous studies have shown that hydrogen-poor SLSNe tend to reside in low-mass galaxies with strong star formation, with the current sample of 31 SLSN-I host galaxies having an average stellar mass ($M_{\rm stellar}$) of $\log(M/{\rm M}_\odot) \approx 8.30$ and an sSFR of $\approx 2\,{\rm Gyr}^{-1}$ (Lunnan et al. 2014). Similar results were found in Perley et al. (2016) with a lower-*z* SLSN-I sample. Here, we examine the properties of the host galaxy of DES15E2mlf.

Using DES images of the host galaxy of DES15E2mlf, we measure *griz* AB magnitudes of 23.46 ± 0.04, 23.30 ± 0.05, 23.47 ± 0.08 and 23.52 ± 0.11 mag, respectively. Fig. 6 shows a DES composite image of the host galaxy and its surrounding field. We also obtain near-infrared (NIR) photometry of the host galaxy from the VISTA Deep Extragalactic Observations (VIDEOs; Jarvis et al. 2013). We measure *ZYJHK*$_{\rm s}$ AB magnitudes of 23.50 ± 0.05, 23.56 ± 0.06, 23.31 ± 0.11, 23.56 ± 0.10, 23.62 ± 0.20 mag, respectively. The addition of NIR photometry is critical for setting more robust constraints on the host-galaxy parameters compared to those obtained from the optical data alone.

Using the photometric redshift code Z-PEG (Le Borgne & Rocca-Volmerange 2002) and assuming a Salpeter (1955) initial mass function (IMF), we measure a stellar mass of $\log(M/{\rm M}_\odot) = 9.54^{+0.31}_{-0.50}$, which is more massive than the typical SLSN-I host galaxy. The photometry also indicates a sSFR of $2.46^{+0.00}_{-1.01}\,{\rm Gyr}^{-1}$. We also notice that the photometric redshift of the host galaxy estimated by Z-PEG changed from 0.2 to 1.9 after including the VIDEO data, which is now consistent with the spectroscopic redshift of the SN. Therefore, this deviation is likely due to the lack of rest-frame optical photometry (note that the DECam photometry of DES15E2mlf are

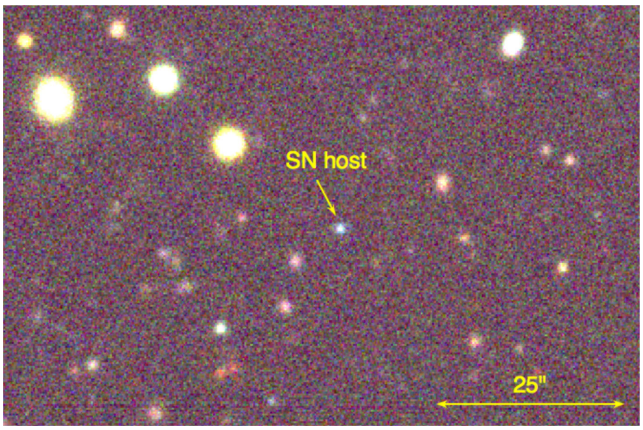

Figure 6. False-colour (RGB channels corresponding to the DECam *irg* filters) template image of the field surrounding DES15E2mlf, with the yellow arrow marking the SN host galaxy. North is up and east is to the left. The host is noticeable blue compared to other objects in the field.

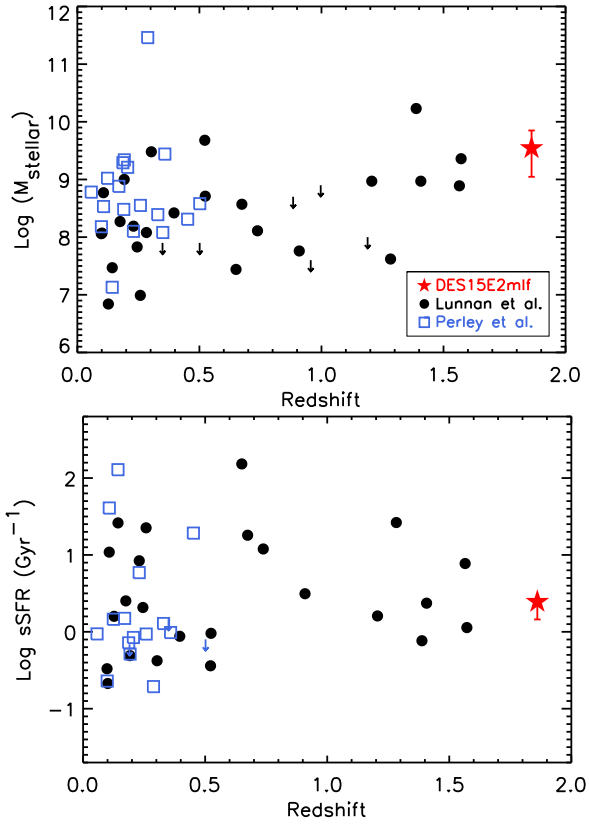

Figure 7. SLSN-I host-galaxy $M_{\rm stellar}$ as a function of redshift (top panel) and sSFR as a function of redshift (bottom panel). Black points and blue squares represent the Lunnan et al. (2014) and Perley et al. (2016) sample, respectively, while the red star represents the host galaxy of DES15E2mlf.

all in rest-frame UV) in estimating the initial photometric redshift of host galaxy.

We present these values compared to those of the Lunnan et al. (2014) and Perley et al. (2016) sample in Fig. 7. Similar stellar population synthesis techniques were used to obtain the host parameters in Lunnan et al. (2014) and Perley et al. (2016). To be consistent, we convert the host stellar mass and SFR to Salpeter IMF if necessary.

DES15E2mlf has one of the most massive host galaxies discovered for an SLSN-I. This continues the trend of increasing stellar mass (on average) with redshift for the Lunnan et al. (2014) sample. Compared to the same sample, the host galaxy of DES15E2mlf has a higher $M_{\rm stellar}$ than 94 per cent (29 out of 31) of all SLSN host galaxies. However, we cannot rule out the possibility that the host is a satellite galaxy with lower $M_{\rm stellar}$.

4 DISCUSSION

4.1 Precursor

Examining the light curves in detail, we notice that the first detection in g, at -21 rest-frame days relative to peak brightness, is $\sim$1 mag brighter than that expected from an extrapolation of the later data. We do not detect any excess flux in other bands at this epoch. A difference of 0.34 ± 0.31 mag is calculated between the first and second detections in g. While this deviation is insignificant ($\sim 1\sigma$) given the photometric uncertainties, it is also potentially consistent with luminous precursor events associated with other SLSNe (e.g. Leloudas et al. 2012; Howell et al. 2013; Nicholl et al. 2015; Smith et al. 2016). These peaks are thought to be related to some shock-heating scenarios (e.g. Piro 2015; Kasen, Metzger & Bildsten 2016), which could provide us critical information of SN progenitor and explosion physics.

Following Nicholl & Smartt (2016), we use the rest-frame g-band light curve of LSQ14bdq (which has a well-sampled precursor) as a template to test the existence of a potential precursor for DES15E2mlf (see Fig. 8). The template is arbitrarily scaled by visual inspection to match the DES15E2mlf g-band light curve. For the *riz* bands, we apply the same temporal scaling factor to the template as in the g band, but arbitrarily scale the flux of the template to match the *riz* light curves.

To match the template to the rising portion of the light curve, the first g-band detection must occur during the declining phase of the precursor. Therefore, because of the lack of good earlier detections, the peak precursor luminosity is limited to $\rm M_{1700\,\text{Å}} < -20.56$ mag (assuming that the first detection is of a precursor). For the *riz* light curves, the templates are either consistent or below the detection limits.

For the epoch of the first detection, we measure colour limits of $g-r<-0.22$, $g-i<-0.01$ and $g-z<0.67$ mag. The $g-r$ colour is particularly constraining for the precursor temperature. Assuming a blackbody, we find that the precursor has $T_{\rm bb} \sim 36\,000$ K, with a lower limit of $\sim$28 500 K (see also Fig 8). This is comparable to temperatures measured for the precursors for other SLSNe (e.g. $T_{\rm bb} \simeq 25\,000 \pm 5000$ K; Nicholl & Smartt 2016).

While our data do not strongly argue for a precursor, they are consistent with such an event.

4.2 Interstellar absorption

Quasars, GRBs and SLSNe are powerful tools in probing the interstellar medium (ISM) of distant galaxies because of their extremely high luminosities. Rao, Turnshek & Nestor (2006) studied a sample of quasars that have intervening Mg II absorption systems. They found the fraction of damped Lyman-α absorbers (DLAs; Wolfe et al. 1986) increased with Mg II EWs. DLAs are characterized by neutral hydrogen gas clouds with a high column density ($\rm N_{H\,I} > 2 \times 10^{20}\,cm^{-2}$). Rao et al. (2006) found that $\sim$36 per cent of all systems with EW(Mg II λ2796) > 0.5 Å and EW(Fe II λ2600) > 0.5 Å are DLAs. The rate increases to

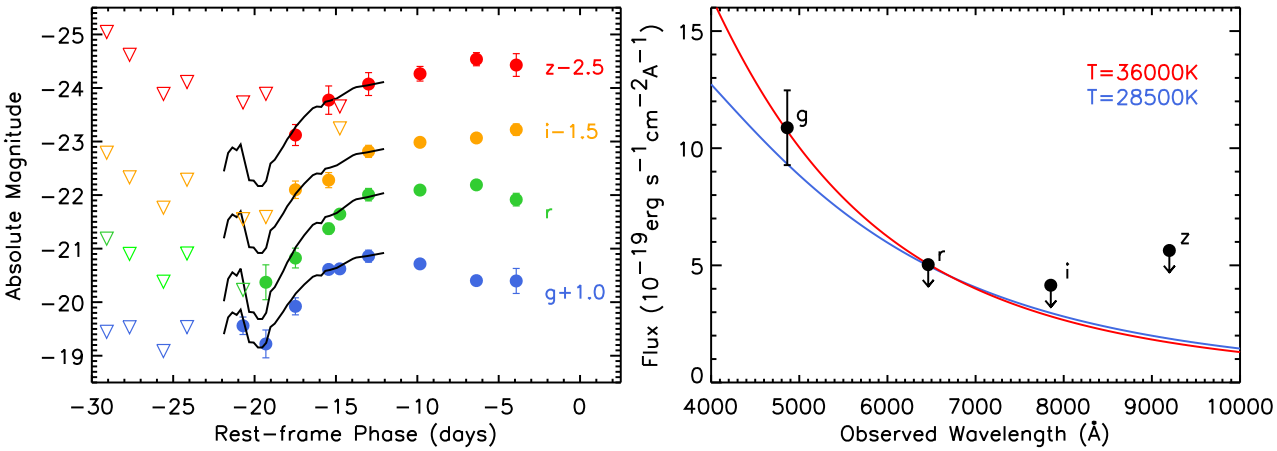

Figure 8. Left-hand panel: A closer look at DES15E2mlf pre-maximum light curves. The upper limits are shown in downward triangles. We overplot the scaled LSQ14bdq rest-frame *g*-band light curve (Nicholl et al. 2015) in black. Right-hand panel: The DES15E2mlf *g*-band flux and upper limits for *riz* bands at −21 d. The blackbody curves with $T = 28\,500$ K (blue) and 36000 K (red) are overplotted.

∼42 per cent with EW(Mg II λ2796)/EW(Fe II λ2600) < 2 and EW(Mg I λ2852) > 0.1 Å, and that essentially no DLAs have EW(Mg II λ2796)/EW(Fe II λ2600) > 2. Therefore, measurements of these absorption features can predict the presence of a DLA.

Examining the narrow absorption lines detected in the spectrum, we measure the rest-frame EWs to be EW(Mg II λ2796) = 2.75 ± 0.04 Å and EW(Mg II λ2803) = 1.83 ± 0.05 Å for DES15E2mlf. However, without the robust detection of Fe II λ2600 and Mg I λ2852 lines, we are not able to constrain an intervening DLA system.

Following Berger et al. (2012), we estimate a lower limit on the column density of $\log N(\mathrm{Mg\,II}) \gtrsim 13.9$. The Mg II EW is higher than that for iPTF13ajg (0.5 Å; Vreeswijk et al. 2014), PS1-11bam (1.3 Å; Berger et al. 2012) and GRB composite spectrum (1.5 Å; Christensen et al. 2011), and even ∼85 per cent of the quasar intervening systems (e.g. Quider et al. 2011). These measurements provide possibilities of using distant SLSNe as probes of ISM from the present all the way back to the early universe.

4.3 Host galaxy and selection bias

We examined the host galaxy of DES15E2mlf, finding it to be higher mass than typical SLSN-I host galaxies. For a large sample of SLSNe-I, the average host-galaxy mass increases with redshift; DES15E2mlf being the highest redshift and having one of the highest mass host galaxies of all SLSNe-I, continues this trend. We now explore some possible explanations.

First, most SLSNe are currently selected by the contrast in brightness between the SN and its host galaxy. Since SLSNe are $\gtrsim$2 mag more luminous at peak than SNe Ia, this strategy is effective at finding particularly luminous SNe and lower luminosity SNe, in particularly, low-luminosity host galaxies. In practice, many SLSN selection techniques prioritize SNe in faint or 'hostless' galaxies (i.e. galaxies below the detection limit of the images; McCrum et al. 2015). As a result, there could be bias against SNe in detected galaxies. The luminosity of a galaxy at the detection limit of a particular survey increases with redshift (i.e. only brighter galaxies can be detected at higher redshift). If SLSN host galaxies have a range of luminosities, a 'hostless' selection criterion would remove SNe with the highest mass host galaxies at lower redshifts. In contrast, those highest mass host galaxies could be selected as hostless events at higher redshift. As a result, the average host-galaxy mass would increase with redshift.

However, Lunnan et al. (2014) found that this potential bias was not significantly affecting the general trend that SLSNe are found in lower luminosity galaxies than other varieties of SNe. Even if the current SLSN sample could be biased to particularly low-luminosity galaxies, there is likely a preference for SLSNe to occur in such galaxies (Lunnan et al. 2014; Perley et al. 2016). None the less, the fact that DES15E2mlf was originally selected as a likely SN Ia at low redshift, but has the higher mass host galaxy of many SLSN-I indicates that this bias certainly has some effect.

While DES15E2mlf had a high-mass host galaxy, it could have had a low-metallicity progenitor; the average metallicity evolves significantly from $z \approx 2$ to 0. To examine this possibility, we estimate the metallicity of the host galaxy of DES15E2mlf using the mass–metallicity relationship (e.g. Tremonti et al. 2004). Since the relationship evolves with redshift (Zahid et al. 2013; Ma et al. 2016), we used the Zahid et al. (2013) parametrization to determine the mass–metallicity relation at $z = 1.861$. With this relation and for the measured M_{stellar} of the host of DES15E2mlf, we estimate that the host-galaxy has a gas-phase metallicity of $12 + \log(\mathrm{O/H}) = 8.72$,[2] which is slightly above the solar value (8.69; Allende Prieto, Lambert & Asplund 2001). Despite the host galaxy's relatively high mass, its metallicity is still ∼0.2 dex lower than that of low-z field galaxies (e.g. Kewley & Ellison 2008) at the same M_{stellar}. A direct measurement would be critical to really constrain the host metallicity of DES15E2mlf.

The detection of an SLSN in a relatively high-mass galaxy suggests that other factors, such as progenitor metallicity, are more important in creating such events. At even higher redshifts, SLSNe may occur at a much higher rate in higher mass galaxies, perhaps providing significant feedback and affecting galaxy formation and evolution. SLSN searches that avoid selection based on host brightness could improve our understanding of this process in high-mass galaxies and at high redshift.

5 CONCLUSIONS

We present the discovery of DES15E2mlf, an SLSN, peaking at $M_{\mathrm{AB}} = -22.3$ mag, discovered in the DES-SN survey at

[2] We used the Kobulnicky & Kewley (2004) metallicity calibration as in Lunnan et al. (2014).

$z = 1.861$. It is the most distant SLSN confirmed to date. Spectroscopic comparisons with other SLSNe indicate that DES15E2mlf is most similar to that of hydrogen-poor SLSNe-I.

While the *riz* light curves evolve similarly, the *g*-band light curve (which corresponds to rest-frame 1700 Å) peaks ∼10 rest-frame days earlier while declining faster and more dramatically than that of the other bands. We find excess flux in the first detection of the *g*-band light curve. This could indicate a potential precursor event similar to that found for many other SLSNe. Compared to other SLSNe, we find that the peak precursor luminosity is limited to $M_{1700Å} < -20.56$ mag. A blackbody temperature $T_{bb} \gtrsim 28\,500$ K is determined for the epoch of the first detection.

We obtained three spectra of DES15E2mlf, covering near-maximum phases (−6 to +8 rest-frame days). The spectra have no strong absorption or emission features between 2300 and 3500 Å, but have two strong absorption features, which were previously identified as Fe III and C III (Howell et al. 2013; Mazzali et al. 2016), at $\lambda \approx 1950$ and 2150 Å, respectively. The wavelength of maximum absorption for each feature shifts to the red with time. Interpreting this as a change in expansion velocity, the velocity decreases by ∼3000–6000 km s^{-1} for the time period covered by our spectra.

We detect strong narrow absorption features, which we interpret as originating in the ISM of the host galaxy. Measuring the EWs of those features, we estimate the column density of the ISM along the line of sight. We find that DES15E2mlf has strong Mg II absorption relative to the average GRB absorbing system and the majority of quasar intervening systems. This shows the possibilities of using distant SLSNe to constrain the gas content of the universe.

We examined the host properties of DES15E2mlf, finding that it has a higher stellar mass than the typical SLSN-I host. We postulate that previous selection algorithms that favoured targeting SNe in faint galaxies could bias the population statistics to lower mass galaxies (at least for the high redshift SN samples) and that DES15E2mlf avoided this potential bias since it was originally targeted as a likely low-redshift SN Ia.

Regardless of a potential selection bias, the host galaxy of DES15E2mlf shows that SLSNe-I can occur in relatively normal galaxies (at least at high redshifts) and likely had a significantly lower metallicity than local galaxies with the same mass. Since DES15E2mlf is the highest redshift SLSN-I known, the high mass of its host galaxy may simply be the result of decreasing metallicity with redshift. A direct metallicity measurement of the host galaxy will result in a more robust conclusion.

Since SLSNe at higher redshift may occur more frequently in higher $M_{stellar}$ galaxies, we suggest the future searches should avoid selecting the candidates based on the brightness of host galaxy. This is especially true for DES, which has become particularly adept at discovering SLSNe at high redshift.

ACKNOWLEDGEMENTS

Y-CP and RJF are supported, in part, by NSF grant AST-1518052. Y-CP thanks T-W Chen for helpful discussions and comments. RJF gratefully acknowledges support from the Alfred P. Sloan Foundation and the David and Lucile Packard Foundation. LG was supported in part by the US National Science Foundation under Grant AST-1311862. MJJ acknowledges support from the UK STFC [ST/N000919/1]. MS acknowledges support from EU/FP7-ERC grant number 615929.

Funding for the DES Projects has been provided by the US Department of Energy, the US National Science Foundation, the Ministry of Science and Education of Spain, the Science and Technology Facilities Council of the United Kingdom, the Higher Education Funding Council for England, the National Center for Supercomputing Applications at the University of Illinois at Urbana-Champaign, the Kavli Institute of Cosmological Physics at the University of Chicago, the Center for Cosmology and Astro-Particle Physics at the Ohio State University, the Mitchell Institute for Fundamental Physics and Astronomy at Texas A&M University, Financiadora de Estudos e Projetos, Fundação Carlos Chagas Filho de Amparo à Pesquisa do Estado do Rio de Janeiro, Conselho Nacional de Desenvolvimento Científico e Tecnológico and the Ministério da Ciência, Tecnologia e Inovação, the Deutsche Forschungsgemeinschaft and the Collaborating Institutions in the Dark Energy Survey.

The Collaborating Institutions are Argonne National Laboratory, the University of California at Santa Cruz, the University of Cambridge, Centro de Investigaciones Energéticas, Medioambientales y Tecnológicas-Madrid, the University of Chicago, University College London, the DES-Brazil Consortium, the University of Edinburgh, the Eidgenössische Technische Hochschule (ETH) Zürich, Fermi National Accelerator Laboratory, the University of Illinois at Urbana-Champaign, the Institut de Ciències de l'Espai (IEEC/CSIC), the Institut de Física d'Altes Energies, Lawrence Berkeley National Laboratory, the Ludwig-Maximilians Universität München and the associated Excellence Cluster Universe, the University of Michigan, the National Optical Astronomy Observatory, the University of Nottingham, The Ohio State University, the University of Pennsylvania, the University of Portsmouth, SLAC National Accelerator Laboratory, Stanford University, the University of Sussex, Texas A&M University, and the OzDES Membership Consortium.

The DES data management system is supported by the National Science Foundation under Grant Number AST-1138766. The DES participants from Spanish institutions are partially supported by MINECO under grants AYA2012-39559, ESP2013-48274, FPA2013-47986 and Centro de Excelencia Severo Ochoa SEV-2012-0234. Research leading to these results has received funding from the European Research Council under the European Unions Seventh Framework Programme (FP7/2007-2013) including ERC grant agreements 240672, 291329 and 306478.

REFERENCES

Allende Prieto C., Lambert D. L., Asplund M., 2001, ApJ, 556, L63
Barkat Z., Rakavy G., Sack N., 1967, Phys. Rev. Lett., 18, 379
Berger E. et al., 2012, ApJ, 755, L29
Bernstein J. P. et al., 2012, ApJ, 753, 152
Blondin S. et al., 2006, AJ, 131, 1648
Bonnett C. et al., 2016, Phys. Rev. D, 94, 042005
Chen T.-W. et al., 2013, ApJ, 763, L28
Chen T.-W. et al., 2015, MNRAS, 452, 1567
Chevalier R. A., Irwin C. M., 2011, ApJ, 729, L6
Chomiuk L. et al., 2011, ApJ, 743, 114
Christensen L., Fynbo J. P. U., Prochaska J. X., Thöne C. C., de Ugarte Postigo A., Jakobsson P., 2011, ApJ, 727, 73
Cooke J. et al., 2012, Nature, 491, 228
Dark Energy Survey Collaboration et al., 2016, MNRAS, 460, 1270
Diehl H. T. et al., 2016, Proc. SPIE Conf. Ser. Vol. 9910, SPIE, Bellingham, p. 99101D
Flaugher B. et al., 2015, AJ, 150, 150
Foley R. J. et al., 2003, PASP, 115, 1220

Gal-Yam A., 2012, Science, 337, 927
Gal-Yam A. et al., 2009, Nature, 462, 624
Ginzburg S., Balberg S., 2012, ApJ, 757, 178
Hook I. M., Jørgensen I., Allington-Smith J. R., Davies R. L., Metcalfe N., Murowinski R. G., Crampton D., 2004, PASP, 116, 425
Howell D. A. et al., 2013, ApJ, 779, 98
Inserra C. et al., 2013, ApJ, 770, 128
Jarvis M. J. et al., 2013, MNRAS, 428, 1281
Kasen D., Bildsten L., 2010, ApJ, 717, 245
Kasen D., Metzger B. D., Bildsten L., 2016, ApJ, 821, 36
Kessler R. et al., 2015, AJ, 150, 172
Kewley L. J., Ellison S. L., 2008, ApJ, 681, 1183
Kobulnicky H. A., Kewley L. J., 2004, ApJ, 617, 240
Le Borgne D., Rocca-Volmerange B., 2002, A&A, 386, 446
Leloudas G. et al., 2012, A&A, 541, A129
Leloudas G. et al., 2015, MNRAS, 449, 917
Lunnan R. et al., 2013, ApJ, 771, 97
Lunnan R. et al., 2014, ApJ, 787, 138
Ma X., Hopkins P. F., Faucher-Giguère C.-A., Zolman N., Muratov A. L., Kereš D., Quataert E., 2016, MNRAS, 456, 2140
Mazzali P. A., Sullivan M., Pian E., Greiner J., Kann D. A., 2016, MNRAS, 458, 3455
McCrum M. et al., 2014, MNRAS, 437, 656
McCrum M. et al., 2015, MNRAS, 448, 1206
Neill J. D. et al., 2011, ApJ, 727, 15
Nicholl M., Smartt S. J., 2016, MNRAS, 457, L79
Nicholl M. et al., 2013, Nature, 502, 346
Nicholl M. et al., 2015, ApJ, 807, L18
Pan Y.-C. et al., 2015, The Astronomer's Telegram, 8460
Papadopoulos A. et al., 2015, MNRAS, 449, 1215
Perley D. A. et al., 2016, ApJ, 830, 14
Piro A. L., 2015, ApJ, 808, L51
Prajs S. et al., 2017, MNRAS, 464, 3568
Quider A. M., Nestor D. B., Turnshek D. A., Rao S. M., Monier E. M., Weyant A. N., Busche J. R., 2011, AJ, 141, 137
Quimby R. M. et al., 2011, Nature, 474, 487
Quimby R. M., Yuan F., Akerlof C., Wheeler J. C., 2013, MNRAS, 431, 912
Rao S. M., Turnshek D. A., Nestor D. B., 2006, ApJ, 636, 610
Sako M. et al., 2008, AJ, 135, 348
Sako M. et al., 2011, ApJ, 738, 162
Salpeter E. E., 1955, ApJ, 121, 161
Saunders W. et al., 2004, in Moorwood A. F. M., Iye M., eds, Proc. SPIE Conf. Ser. Vol. 5492, Ground-based Instrumentation for Astronomy, SPIE, Bellingham, p. 389
Schlafly E. F., Finkbeiner D. P., 2011, ApJ, 737, 103
Silverman J. M. et al., 2012, MNRAS, 425, 1789
Smith N. et al., 2007, ApJ, 666, 1116
Smith M. et al., 2016, ApJ, 818, L8
Tremonti C. A. et al., 2004, ApJ, 613, 898
Vreeswijk P. M. et al., 2014, ApJ, 797, 24
Wade R. A., Horne K., 1988, ApJ, 324, 411
Wolfe A. M., Turnshek D. A., Smith H. E., Cohen R. D., 1986, ApJS, 61, 249
Woosley S. E., 2010, ApJ, 719, L204
Zahid H. J., Geller M. J., Kewley L. J., Hwang H. S., Fabricant D. G., Kurtz M. J., 2013, ApJ, 771, L19

[1]*Department of Astronomy and Astrophysics, University of California, Santa Cruz, CA 95064, USA*
[2]*Department of Physics and Astronomy, University of Southampton, Southampton, Hampshire SO17 1BJ, UK*
[3]*Pittsburgh Particle Physics, Astrophysics, and Cosmology Center (PITT PACC), Pittsburgh, PA 15260, USA*
[4]*Physics and Astronomy Department, University of Pittsburgh, Pittsburgh, PA 15260, USA*
[5]*Institute of Cosmology and Gravitation, Dennis Sciama Building, University of Portsmouth, Burnaby Road, Portsmouth PO1 3FX, UK*
[6]*Center for Mathematical Modelling, University of Chile, Beauchef 851, Santiago, Chile*
[7]*Millennium Institute of Astrophysics, Universidad de Chile, Casilla 36-D, Santiago, Chile*
[8]*Astrophysics, The Denys Wilkinson Building, University of Oxford, Keble Road, Oxford OX1 3RH, UK*
[9]*Department of Physics, University of the Western Cape, Bellville 7535, South Africa*
[10]*Kavli Institute for Cosmological Physics, University of Chicago, Chicago, IL 60637, USA*
[11]*Department of Astronomy and Astrophysics, University of Chicago, 5640 South Ellis Avenue, Chicago, IL 60637, USA*
[12]*Argonne National Laboratory, 9700 South Cass Avenue, Lemont, IL 60439, USA*
[13]*Australian Astronomical Observatory, North Ryde, NSW 2113, Australia*
[14]*School of Sciences, European University Cyprus, 6 Diogenis Str., Engomi, 1516 Nicosia, Cyprus*
[15]*Department of Physics and Astronomy, University of Pennsylvania 209 South 33rd Street, Philadelphia, PA 19104, USA*
[16]*Cerro Tololo Inter-American Observatory, National Optical Astronomy Observatory, Casilla 603, La Serena, Chile*
[17]*Department of Physics and Astronomy, University College London, Gower Street, London WC1E 6BT, UK*
[18]*Department of Physics and Electronics, Rhodes University, PO Box 94, Grahamstown 6140, South Africa*
[19]*Fermi National Accelerator Laboratory, PO Box 500, Batavia, IL 60510, USA*
[20]*LSST, 933 North Cherry Avenue, Tucson, AZ 85721, USA*
[21]*CNRS, UMR 7095, Institut d'Astrophysique de Paris, F-75014, Paris, France*
[22]*Sorbonne Universités, UPMC Univ Paris 06, UMR 7095, Institut d'Astrophysique de Paris, F-75014, Paris, France*
[23]*Kavli Institute for Particle Astrophysics and Cosmology, PO Box 2450, Stanford University, Stanford, CA 94305, USA*
[24]*SLAC National Accelerator Laboratory, Menlo Park, CA 94025, USA*
[25]*Laboratório Interinstitucional de e-Astronomia - LIneA, Rua Gal. José Cristino 77, Rio de Janeiro, RJ - 20921-400, Brazil*
[26]*Observatório Nacional, Rua Gal. José Cristino 77, Rio de Janeiro, RJ - 20921-400, Brazil*
[27]*Department of Astronomy, University of Illinois, 1002 W. Green Street, Urbana, IL 61801, USA*
[28]*National Center for Supercomputing Applications, 1205 West Clark St., Urbana, IL 61801, USA*
[29]*Institut de Ciències de l'Espai, IEEC-CSIC, Campus UAB, Carrer de Can Magrans, s/n, E-08193 Bellaterra, Barcelona, Spain*
[30]*Institut de Física d'Altes Energies (IFAE), The Barcelona Institute of Science and Technology, Campus UAB, E-08193 Bellaterra, Spain*
[31]*Department of Physics, IIT Hyderabad, Kandi, Telangana 502285, India*
[32]*Jet Propulsion Laboratory, California Institute of Technology, 4800 Oak Grove Dr., Pasadena, CA 91109, USA*
[33]*Instituto de Fisica Teorica UAM/CSIC, Universidad Autonoma de Madrid, E-28049 Madrid, Spain*
[34]*Department of Astronomy, University of California, Berkeley, 501 Campbell Hall, Berkeley, CA 94720, USA*
[35]*Lawrence Berkeley National Laboratory, 1 Cyclotron Road, Berkeley, CA 94720, USA*
[36]*Astronomy Department, University of Washington, Box 351580, Seattle, WA 98195, USA*
[37]*Departamento de Física Matemática, Instituto de Física, Universidade de São Paulo, CP 66318, CEP 05314-970, São Paulo, SP, Brazil*
[38]*George P. and Cynthia Woods Mitchell Institute for Fundamental Physics and Astronomy, Texas A&M University, TX 77843, USA*
[39]*Center for Cosmology and Astro-Particle Physics, The Ohio State University, Columbus, OH 43210, USA*
[40]*Department of Astronomy, The Ohio State University, Columbus, OH 43210, USA*

[41] *Institució Catalana de Recerca i Estudis Avançats, E-08010 Barcelona, Spain*
[42] *Department of Physics and Astronomy, Pevensey Building, University of Sussex, Brighton BN1 9QH, UK*
[43] *Centro de Investigaciones Energéticas, Medioambientales y Tecnológicas (CIEMAT), E-28040 Madrid, Spain*
[44] *Department of Physics, University of Michigan, Ann Arbor, MI 48109, USA*
[45] *Universidade Federal do ABC, Centro de Ciências Naturais e Humanas, Av. dos Estados, 5001, Santo André, 09210-580 SP, Brazil*
[46] *Computer Science and Mathematics Division, Oak Ridge National Laboratory, Oak Ridge, TN 37831, USA*

This paper has been typeset from a TEX/LATEX file prepared by the author.